Laser-assisted Preparation of C_3N_4/Fe_2O_3/Au Nanocomposite: A Magnetic Reusable Catalyst for Pollutant Degradation

Atefeh Nasri
Bu Ali sina university
Zahra Nezafat
University of Qom
Babak Jaleh (jaleh@basu.ac.ir)
Bu Ali Sina University
Yasin Orooji
Nanjing Forestry University
Rajender S. Varma
Palacky University Olomouc: Univerzita Palackeho v Olomouci

Research Article

Keywords: C3N4/Fe2O3/Au nanocomposite, Reduction, 4-Nitrophenol, Dye, Laser ablation

Posted Date: February 17th, 2021

DOI: https://doi.org/10.21203/rs.3.rs-180701/v1

Version of Record: A version of this preprint was published at Clean Technologies and Environmental Policy on March 14th, 2021. See the published version at https://doi.org/10.1007/s10098-021-02065-4.

Abstract

Assorted common contaminants namely organic dyes and nitro compounds are generated by various industries and have caused alarming problems for the environment and humans. The development of effective and newer methods to eliminate these contaminants is imperative. One effective way to eliminate these pollutants is to deploy sustainable heterogeneous catalyst systems. Accordingly, a novel and efficient magnetic nanocomposite catalyst comprising graphitic carbon nitride (g-C_3N_4), gold (Au), and hematite (α-Fe_2O_3) nanoparticles (C_3N_4/Fe_2O_3/Au) is prepared through a cost-effective and green method. The individual components, g-C_3N_4 and Au nanoparticles (NPs), are prepared via thermal decomposition of urea and laser ablation in liquid (LAL), respectively. The behavior of C_3N_4/Fe_2O_3/Au nanocomposite as a catalyst for the borohydride reduction of methyl orange (MO) dye and 4-nitrophenol (4-NP) in aqueous solution is illustrated.

1. Introduction

Semiconductor materials are among the most promising catalysts for the degradation of the organic contaminants in view of their inexpensive nature, outstanding stability, and easy separation (Liang et al. 2017). Metal free g-C_3N_4, one of the polymeric semiconductor materials, has a layered structure with tri-s-triazine units comprising nitrogen and carbon elements in each layer (Niu et al. 2012). Surface properties and existence of basic sites in g-C_3N_4 are largely responsible for this polymer to gain more attention in many applications such as catalysis (Zhu et al. 2014). g-C_3N_4 has prominent features namely attractive electronic structure (band gap 2.7 eV), great thermal stability, and surface area, easy accessibility via facile synthesis methods such as thermal decomposition of earth-abundant, low cost, and nitrogen rich raw materials e.g. cyanamide, dicyandiamide, melamine, thiourea and urea (Liu et al. 2020; Majumdar and Pal 2020; Ong et al. 2016). Urea is a suitable precursor to fabricate the g-C_3N_4 with high porosity and great surface area (Ong et al. 2016; Zhang et al. 2012). However, numerous attempts are made to modify g-C_3N_4's catalytic performance due to some of its natural limitations. For instance, deposition of some metallic NPs such as Pd, Pt, Ag, Au, TiO_2 and ZnO on surface of g-C_3N_4 can improve its catalytic activities (Ding et al. 2017; Zhu et al. 2014). One of the metal NPs with high conductivity and low toxicity is Au NPs which was used in many fields for example, electronics, optics, biomedicine, and catalyst (Nasri et al. 2020; Yang et al. 2015).

By using toxic reducing agents and surfactants, chemical methods are widely deployed to fabricate NPs, which can be dangerous for environment and human health. LAL technique is a greener, inexpensive, and a fast protocol for the production of NPs within minutes (Mohazzab et al. 2019a; Mohazzab et al. 2019b; Mohazzab et al. 2020; Jaleh et al. 2020b; Zhang et al. 2017).

The deployment of heterogeneous catalysts in various chemical transformations is of great interest to researchers (Habibi et al. 2011, 2013). Among the many benefits, the most important one being their easy separation from the reaction mixture (Orooji et al. 2020; Salavati-Niasari and Banitaba 2003; Salavati-

Niasari et al. 2004, 2008). Nanocatalysts (Salavati-Niasari 2005; Salavati-Niasari et al. 2009a; b) are significant materials which have demonstrated their prowess in chemical processes and remediation of environmental pollutants. The green synthesized nanocatalysts with features namely large surface area, good thermal tenacity and biocompability, and simple separation of reaction mixtures are suitable for solving the environmental problems. The magnetic iron oxide-based nanocatalysts, such as magnetite (Fe_3O_4), hematite (α-Fe_2O_3) (Esmaeili et al. 2011), and maghemite (γ-Fe_2O_3) nanocatalysts, endowed with good biocompatibility, low toxicity, and eco-friendly properties, are attractive in catalytic processes due to their fast and cost effective separation by exerting an external magnetic field with less waste and consumption of the catalyst (Jaleh et al. 2017; Jiang et al. 2017; Tayel et al. 2019; Wang et al. 2015b; Zhuang et al. 2017). Hematite (α-Fe_2O_3), a low cost, earth-abundant, and thermodynamically stable material with narrow band gaps, has been mostly used as a support for metal NPs to improve its catalytic performance (Han et al. 2019a).

Organic dyes and nitro compounds are harmful substances that enter water bodies and the environment from various industries such as textiles, leather, printing and pharmaceuticals (Jaleh et al. 2020a; Nasrollahzadeh et al. 2020b; 2020c; Zhu et al. 2011). Due to the great stability and solvability of nitro compounds, especially 4-nitrophenol (4-NP), they are dangerous contaminants in water. To date, many efforts have been made to remove organic dyes and 4-NP from the environment using assorted techniques such as microbiological discoloration, physical adsorption, electrochemical treatment, and chemical coagulation for the elimination of these contaminants from water and environment (Canizares et al. 2004; Cervantes and Dos Santos 2011; El-Gohary and Tawfik 2009; Lucarelli et al. 2000; Zhu et al. 2011). Nevertheless, they suffer from several shortcomings namely severe conditions, being expensive and the microorganisms elimination from destroyed entities that limit their use (Nasrollahzadeh et al. 2020c). Therefore, the use of effective catalysts generated by cleaner means is significant (Balakumar et al. 2020; Dat et al. 2020; Islam et al. 2018; Jia et al. 2019; Nasrollahzadeh et al. 2020a); some studies have applied photocatalytic systems for dyes degradation (Ghanbari and Salavati-Niasari 2018; Karami et al. 2020; Nasrollahzadeh et al. 2018). In fact, catalytic reduction of pollutants by suitable catalysts and $NaBH_4$ is one of the best possible pathways to remove these contaminants, because it has many advantages encompassing efficient operation, easy reaction conditions, and reasonable price.

Herein, we present an effective protocol for the production of C_3N_4/Fe_2O_3/Au nanocomposite by a simple technique and the appliance of this nanocomposite for the borohydride reduction of MO and 4-NP is described.

2. Experimental

2.1 Materials and tools

Urea (CAS NO. 57-13-6), methanol (CH_3OH, CAS NO. 67-56-1) and ethanol (C_2H_5OH, CAS NO. 64-17-5) were procured from Merck Chemical Company. sodium hydroxide (NaOH, ≥ 98%), iron(III) nitrate

nonahydrate ($Fe(NO_3)_3.9H_2O$, ≥ 98%), 4-nitrophenol, methyl orange, sodium borohydride and *n*-propyl amine (CH_3-$(CH_2)_2$-NH_2, 97%) were procured from Sigma-Aldrich Company. UV-Vis spectra were recorded on a Hitachi U-2900 instrument. All solutions were prepared with deionized water. A gold plaque (99.99%) was utilized as a target for LAL process and Au NPs synthesis. To study the morphology and structure of the nanocomposite, X-ray diffraction (XRD, ADP2000), Fourier transform infrared (FTIR, Thermo Nicolet, via KBr pellets), field emission scanning electron microscopy (FESEM, TESCAN-MIRA3-XMU), energy dispersive X-ray spectrometry (EDX, TESCAN-MIRA3-XMU), Brunauer-Emmett-Teller (BET, BELSORP-mini II) and Barret-Joyner-Halenda (BJH) analyses were employed. The magnetic feature of the nanocomposite was perused by vibrating sample magnetometer (VSM, MDKFT).

2.2 Fabrication of g-C_3N_4

g-C_3N_4 was fabricated via thermal decomposition of urea. Briefly, urea (10 g) was heated in a covered capped crucible at 550°C at a temperature gradient of 5°C/min for 3 h. Then, the crucible was cooled and taken out. The obtained yellowish product was g-C_3N_4. The weight of the yellowish powders was 0.45 g (Nasri et al. 2020).

2.3 Synthesis of Fe_2O_3 nanoparticles

To fabricate the α-Fe_2O_3 NPs, 0.03 M $Fe(NO_3)_3.9H_2O$ was stirred and mixed with 20% *n*-propyl amine in methanol, resulting in a brownish solution. After addition of 0.1 M NaOH to the solution and stirring again, a pH meter was used to determine the pH of resultant solution which reached 12. After that, the solution was heated at 90°C for 1 h in a two-necked glass pot and a dark brown solution was obtained. To separate the particles, the solution was centrifuged at 3000 rpm min^{-1} up to 5 min and then washed by methanol, acetone, and ethanol and dried (Wahab et al. 2018).

2.4 Synthesis of $C_3N_4/Fe_2O_3/Au$

The colloidal suspension of Au NPs was prepared using the fiber laser (1064 nm, RFLP30Q) highest output of 30W. A cleaned gold plate was first soaked in a glass dish, with deionized water (~ 5 mL). The laser beam, having a laser pulse length of 100 ns, the frequency of 20 KHz, and scanning pace of 200 mm/s was focused on to the gold plate from above (perpendicularly onto the target) (Mohazzab et al. 2019b). The area of the irradiation beam was 10 mm × 10 mm. The ablation time of the gold target was about 6 min. During the LAL process, the color of liquid changed to red, illustrating the production of Au NPs. The produced colloidal Au NPs was transferred to a separate vessel, stopping the laser irradiation every one minutes due to the absorption of laser light by nanoparticles and avoiding the possibility of particle aggregation.

To prepare $C_3N_4/Fe_2O_3/Au$, C_3N_4 (0.2g) was scattered ultrasonically in 60 mL ethanol/water (2:1) mixture for 3 h under ambient condition. After that, 0.2 g of Fe_2O_3 NPs was added to it and dispersed for 1 more hour and vigorously stirred nonstop for 5 h. Colloidal Au NPs and C_3N_4/Fe_2O_3 solution were subsequently blended and stirred overnight. Finally, $C_3N_4/Fe_2O_3/Au$ nanocomposite was segregated and desiccated.

2.5 C_3N_4/Fe_2O_3/Au catalyzed reduction of 4-NP

A $NaBH_4$ solution (0.25 M) was introduced to a mixture of 4-NP (25 mL, 2.5× 10^{-3} M) and 10.0 mg of C_3N_4/Fe_2O_3/Au and blended under ambient temperature. The disappearance of the yellowish coloration indicates a reduction of 4-NP to 4-aminophenol (4-AP) and the completion of the outcome was tracked by UV-vis spectroscopy

2.6 C_3N_4/Fe_2O_3/Au catalyzed reduction of MO

To a mixture of MO solution (25 mL, 3 × 10^{-3} M) and 10.0 mg of C_3N_4/Fe_2O_3/Au, a $NaBH_4$ solution (5.3 × 10^{-3} M) were introduced and blended at ambient temperature. The reaction advancement was followed through UV-vis spectroscopy. When the orange color of the reaction mixture becomes colorless, MO reduction reaction is considered visibly completed.

3. Results And Discussion

3.1 Characterization of C_3N_4/Fe_2O_3/Au structure

XRD technique was utilized to investigate the nanocomposite structure. The XRD pattern of pure C_3N_4 in Fig. 1a shows two diffraction peaks at Bragg angles 2θ 13.1° (100) and 27.6° (002) (JCPDS 87-1526). The former is ascribed to the repeated structural packing of the heptazine network and the latter corresponds to the regular graphite-like interlayer stacking (Liu et al. 2011). The diffraction peaks at Bragg angles 2θ 24.1° (012), 33.1° (104), 35.6° (110), 40.9° (113), 43.3° (202), 49.5° (024), 54.0° (116), 57.6° (018), 62.1° (214), 63.7° (300), 69.7° (208), 72.0° (1010), and 75.7° (220) can be indexed as hematite (α-Fe_2O_3) in the Fig. 1b (JCPDC 39-1346) (Wahab et al. 2018). The XRD pattern of C_3N_4/Fe_2O_3/Au nanocomposite (Fig. 1c) demonstrates diffraction peaks at around 38.1° (111), 44.4° (200), 64.7° (220), 77.5° (311), and 81.5° (222),corresponding to the Au NPs (JCPDS 00-004-0784) (Kumar et al. 2014). Figure 1c confirms the presence of C_3N_4, Fe_2O_3 and Au NPs and formation of the nanocomposite. The peak intensities of C_3N_4 are weaker, which can be due to the intercalation of nanoparticles into the layers of the C_3N_4. According to the Scherrer's equation (Venkateswarlu et al. 2010), the crystallite sizes of the Fe_2O_3 and Au NPs were calculated and found to be 29.87 and 22.52 nm, respectively.

The FTIR measurement was performed to investigate the nanocomposite structure and chemical functional groups. The spectra of C_3N_4, α-Fe_2O_3, and C_3N_4/Fe_2O_3/Au nanocomposite are depicted in Fig. 2. The band, appeared from 3000–3300 cm^{-1} is imputed to stretching modes of the incomplete condensed amino groups (-NH_2 and -NH) (Alizadeh et al. 2019). The bands in 1246–1636 cm^{-1} range are attributed to the bonding mode of C_3N_4 heterocycles. The peaks at 1246, 1325, and 1415 cm^{-1} are owned by the C-N band and the peaks at nearly 1573 and 1636 cm^{-1} are owned by the C = N band

(Gonçalves et al. 2018). The peak at 811 cm^{-1} corresponds to the condensed C_3N_4 heterocycles and is due to the breathing mode of heptazine ring units (Wang et al. 2015a). The peaks about 481 and 562 cm^{-1} are related to Fe-O stretch of Fe_2O_3 (Han et al. 2019b). There is no obvious peak, indicating a chemical bond between Au and C_3N_4.

The morphology of $C_3N_4/Fe_2O_3/Au$ was evaluated by FESEM analysis. The wrinkled nanosheets and two-dimensional aggregated lamellar structure of C_3N_4 are visible in Fig. 3. The Fig. 3b indicates the deposition of spherical Au NPs on the surface of C_3N_4 nanosheets. Moreover, Fe_2O_3 NPs were detected in Fig. 3c. Due to magnetic attraction among Fe_2O_3 NPs, some agglomeration was observed in the nanocomposite.

EDX, elemental analysis was employed to determine the component contents. The resultant spectrum of $C_3N_4/Fe_2O_3/Au$ nanocomposite was shown in Fig. 4. This pattern indicates the existence of carbon, nitrogen, oxygen, iron and gold, confirming the formation of $C_3N_4/Fe_2O_3/Au$. The atomic percentage of elements are listed in the Fig. 4.

The desorption/adsorption of N_2 at 77 K on the surface of the $C_3N_4/Fe_2O_3/Au$ was accomplished to assess the pore structure and the specific surface area of samples. Figure 5a present the N_2 adsorption/desorption isotherms with a hysteresis loop which shows the presence of mesopores in sample; pore size distribution of sample was calculated (Fig. 5b) using BJH method, most abundant pore diameter of sample being 1.6 nm. The BET surface area, mean pore diameter and pore volume are 25.2 $m^2\ g^{-1}$, 32.1 nm, and0.2 $cm^3\ g^{-1}$, respectively. The calculated structural parameters indicate that $C_3N_4/Fe_2O_3/Au$ has a huge surface area.

Magnetization measurements were performed using VSM analysis under ambient condition. The magnetic hysteresis loop of the $C_3N_4/Fe_2O_3/Au$ nanocomposite, sweeping from − 10000 to 10000 Oe magnetic field, is depicted in Fig. 6; the nanocomposite has a S-like magnetization hysteresis loop and ferromagnetic behaviour. The saturation magnetization (M_s) and remnant magnetization (M_r) are 8.32 and 1.56 emu/g, respectively with coercivity (H_c) of 200 Oe.

3.2 Catalytic reduction of 4-NP

To examine the catalytic performance of $C_3N_4/Fe_2O_3/Au$, the reduction of 4-NP was undertaken in the attendance of $NaBH_4$ (Scheme 1). The reaction advancement was determined with UV-vis spectroscopy (Fig. 7); 4-NP has an absorption band peak of about 300 nm. When $NaBH_4$ solution is added, wavelength increases from 300 nm to 400 nm in view of the 4-nitrophenolate (4-NPT) ion formation. Then, by supplementing 10.0 mg $C_3N_4/Fe_2O_3/Au$ nanocomposite, the absorption band of about 400 nm was reduced until it disappeared after 10 minutes. Finally, a novel absorption band of about 300 nm is observed, that confirmed the 4-AP formation. Table 1 shows the effect of different amounts of catalyst;

best results were obtained with 10.0 mg of the catalyst, with a reduction reaction occurring within 10 min (entry 3).

Table 1.

Reduction of 4-NP using various amount of catalyst.

Entry	C_3N_4/Fe_2O_3/Au nanocomposite (mg)	Time (min)
1	5.0	32
2	7.0	17
3	10.0	10

The mechanism proposed for the catalytic reduction of 4-NP is depicted in Scheme 2 which occurs over an electron transfer reaction (Hatamifard et al. 2015; Bordbar et al. 2018). After adding the $NaBH_4$, BH_4^- ion and 4-NP, they are attached to the C_3N_4/Fe_2O_3/Au nanocomposite surface by electrostatic attraction. The Au NPs in nanocomposite play a significant function for the catalytic reduction of 4-NP and actually serve as an electron transfer system among the BH_4^- donor and nitro group acceptor. Lastly, the 4-NP is transformed to 4-AP by nitrophenolate intermediate and the catalytic run takes place again.

3.3 Reduction of MO by C_3N_4/Fe_2O_3/Au

We also considered the MO reduction reaction at room temperature (Scheme 3). The catalytic reduction of MO deploying 10.0 mg C_3N_4/Fe_2O_3/Au nanocomposite and solution of $NaBH_4$ occurs within 3 min and the advancement of the reaction is monitored by UV-vis spectroscopy (Fig. 8); the solution of MO in water has a peak at λ_{max} 465 nm. Before addition of the C_3N_4/Fe_2O_3/Au nanocomposite to the reaction mixture, the absorption spectrum does not show any change, but after addition, the reaction mixture becomes colorless as the MO reduction occurs. Table 2 shows the catalytic reduction of MO using varying amounts of C_3N_4/Fe_2O_3/Au nanocomposite and $NaBH_4$ solution in water(5.3×10^{-3} M) at ambient temperature. The optimum catalytic reduction of MO was observed by using 10.0 mg of C_3N_4/Fe_2O_3/Au and 25 mL of $NaBH_4$ (5.3×10^{-3} M) at ambient temperature within 3 minutes (entry 3).

Table 2.

Catalytic reduction of MO deploying various amount of catalyst.

Entry	C_3N_4/Fe_2O_3/Au nanocomposite (mg)	Time (min)
1	5.0	15
2	7.0	5
3	10.0	3

4. Recyclability Of Catalyst

One of the important advantages of magnetic catalysts is its easy partitioning from the mixture. We used the reduction of 4-NP as a model reaction. After completing the reaction in the first run, the catalyst was removed by using an external magnet, washed with water, dried, and used for the following cycle. The result exhibited that the catalyst can be retrieved for five times and reused with no noticeable performance loss. As depicted in Fig. 9, a minor decline in the yield occurred subsequent to the fifth cycle but the heterogeneous nature and the recyclability potential of the catalyst was discerned.

5. Conclusion

In summary, the C_3N_4/Fe_2O_3/Au nanocomposite was synthesized using an efficient and straightforward pathway. For the synthesis of Au NPs, greener LAL technique was used and carbon-based g-C_3N_4 was synthesized by pyrolysis of urea. The XRD, FTIR, FESEM, EDX and VSM confirmed the fabrication of C_3N_4/Fe_2O_3/Au nanocomposite. The prepared C_3N_4/Fe_2O_3/Au nanocomposite has a high performance for catalytic reduction of 4-NP and MO in water. The synthesized C_3N_4/Fe_2O_3/Au nanocomposite can be reused for five cycles without noteworthy loss of performance. This general and sustainable approach deploying earth-abundant materials may be adapted for the degradation of other dyestuff in water bodies.

Declarations

Acknowledgments

We appreciate the supports rendered by Bu-Ali Sina University and Nanjing Forestry University [Grant Nos. 163020211 and 163020210], and Symbolic Achievement Cultivation Project [grant number 163020139].

Conflict of Interest: Authors declare no conflict of interest.

References

1. Alizadeh T, Nayeri S, Hamidi N (2019) Graphitic carbon nitride (g-C_3N_4)/graphite nanocomposite as an extraordinarily sensitive sensor for sub-micromolar detection of oxalic acid in biological samples. RSC adv 9:13096-13103. https://doi.org/10.1039/C9RA00982E

2. Balakumar V, Kim H, Ryu JW, Manivannan R, Son Y-A (2020) Uniform assembly of gold nanoparticles on s-doped g-C_3N_4 nanocomposite for effective conversion of 4-nitrophenol by catalytic reduction. J Mater Sci Technol 40:176-184. https://doi.org/10.1016/j.jmst.2019.08.031
3. Bordbar M, Negahdar N, Nasrollahzadeh M (2018) *Melissa Officinalis* L. leaf extract assisted green synthesis of CuO/ZnO nanocomposite for the reduction of 4-nitrophenol and Rhodamine B. Sep Purif Technol 191:295-300. https://doi.org/10.1016/j.seppur.2017.09.044
4. Canizares P, Saez C, Lobato J, Rodrigo M (2004) Electrochemical treatment of 4-nitrophenol-containing aqueous wastes using boron-doped diamond anodes. Ind Eng Chem Res 43:1944-1951. https://doi.org/10.1021/ie034025t
5. Cervantes FJ, Dos Santos AB (2011) Reduction of azo dyes by anaerobic bacteria: microbiological and biochemical aspects. Environ Sci Biotechnol 10:125-137. https://doi.org/10.1007/s11157-011-9228-9
6. Dat NM, Long PNB, Nhi DCU, Minh NN, Nam HM, Phong MT, Hieu NH (2020) Synthesis of silver/reduced graphene oxide for antibacterial activity and catalytic reduction of organic dyes. Synth Met 260:116260. https://doi.org/10.1016/j.synthmet.2019.116260
7. Ding F, Yang D, Tong Z, Nan Y, Wang Y, Zou X, Jiang Z (2017) Graphitic carbon nitride-based nanocomposites as visible-light driven photocatalysts for environmental purification. Environ Sci Nano 4:1455-1469. https://doi.org/10.1039/C7EN00255F
8. El-Gohary F, Tawfik A (2009) Decolorization and COD reduction of disperse and reactive dyes wastewater using chemical-coagulation followed by sequential batch reactor (SBR) process. Desalination 249:1159-1164. https://doi.org/10.1016/j.desal.2009.05.010
9. Esmaeili E, Salavati-Niasari M, Mohandes F, Davar F, Seyghalkar H (2011) Modified single-phase hematite nanoparticles via a facile approach for large-scale synthesis. Chem Eng J 170:278-285. https://doi.org/10.1016/j.cej.2011.03.010
10. Ghanbari M, Salavati-Niasari M (2018) Tl_4CdI_6 nanostructures: facile sonochemical synthesis and photocatalytic activity for removal of organic dyes. Inorg chem 57:11443-11455. https://doi.org/10.1021/acs.inorgchem.8b01293
11. Gonçalves R, Lima TM, Paixão MW, Pereira EC (2018) Pristine carbon nitride as active material for high-performance metal-free supercapacitors: simple, easy and cheap. RSC adv 8:35327-35336. https://doi.org/10.1039/C8RA06656F
12. Habibi D, Nasrollahzadeh M, Bayat Y (2011) $AlCl_3$ as an effective lewis acid for the synthesis of arylaminotetrazoles. Synth Commun 41(14):2135-2145. https://doi.org/10.1080/00397911.2010.497728
13. Habibi D, Nasrollahzadeh M, Sahebekhtiari H (2013) Green synthesis of formamides using the Natrolite zeolite as a natural, efficient and recyclable catalyst. J Mol Catal A Chem 378:148-155. https://doi.org/10.1016/j.molcata.2013.04.001
14. Han Q, Zhang D, Guo J, Zhu B, Huang W, Zhang S (2019a) Improved Catalytic Performance of Au/α-Fe_2O_3-Like-Worm Catalyst for Low Temperature CO Oxidation. Nanomaterials 9:1118.

https://doi.org/10.3390/nano9081118

15. Han T, Wei Y, Jin X, Jiu H, Zhang L, Sun Y, Tian J, Shang R, Hang D, Zhao R (2019b) Hydrothermal self-assembly of α-Fe_2O_3 nanorings@ graphene aerogel composites for enhanced Li storage performance. J Mater Sci 54:7119-7130. https://doi.org/10.1007/s10853-019-03371-5
16. Islam MT, Saenz-Arana R, Wang H, Bernal R, Noveron JC (2018) Green synthesis of gold, silver, platinum, and palladium nanoparticles reduced and stabilized by sodium rhodizonate and their catalytic reduction of 4-nitrophenol and methyl orange. New J Chem 42:6472-6478. https://doi.org/10.1039/C8NJ01223G
17. Jaleh B, Karami S, Sajjadi M, Mohazzab BF, Azizian S, Nasrollahzadeh M, Varma RS (2020) Laser-assisted preparation of Pd nanoparticles on carbon cloth for the degradation of environmental pollutants in aqueous medium. Chemosphere 246:125755. https://doi.org/10.1016/j.chemosphere.2019.125755
18. Jaleh B, Khalilipour A, Habibi S, Niyaifar M, Nasrollahzadeh M (2017) Synthesis, characterization, magnetic and catalytic properties of graphene oxide/Fe_3O_4. J Mater Sci Mater Electron 28:4974-4983. https://doi.org/10.1007/s10854-016-6151-4
19. Jaleh B, Nasrollahzadeh M, Mohazzab BF, Eslamipanah M, Sajjadi M, Ghafuri H (2020b) State-of-the-art technology: Recent investigations on laser-mediated synthesis of nanocomposites for environmental remediation. https://doi.org/10.1016/j.ceramint.2020.12.197
20. Jia X, Ma Y, Liu Y, Wang Y, Zhang Q (2019) Silver nanoparticles decorated by amino groups on the periphery of litchi-like P (MMA-AA-DVB)@ Fe_3O_4 microspheres for the catalytic reduction of methyl orange. Catal Letters 149:2873-2886. https://doi.org/10.1007/s10562-019-02823-6
21. Jiang X, Li L, Cui Y, Cui F (2017) New branch on old tree: green-synthesized RGO/Fe_3O_4 composite as a photo-Fenton catalyst for rapid decomposition of methylene blue. Ceram Int 43:14361-14368. https://doi.org/10.1016/j.ceramint.2017.07.195
22. Karami M, Ghanbari M, Amiri O, Salavati-Niasari M (2020) Enhanced antibacterial activity and photocatalytic degradation of organic dyes under visible light using cesium lead iodide perovskite nanostructures prepared by hydrothermal method. Sep and Purif Technol 253:117526. https://doi.org/10.1016/j.seppur.2020.117526
23. Kumar A, De A, Saxena A, Mozumdar S (2014) Environmentally benign synthesis of positively charged, ultra-low sized colloidal gold in universal solvent. Adv Nat Sci-Nanosci 5:025017. https://doi.org/10.1088/2043-6262/5/2/025017
24. Liang Q, Yu L, Jiang W, Zhou S, Zhong S (2017) One-pot synthesis of magnetic graphitic carbon nitride photocatalyst with synergistic catalytic performance under visible-light irradiation. J Photochem Photobiol A 335:165-173. https://doi.org/10.1016/j.jphotochem.2016.11.012
25. Liu J, Zhang T, Wang Z, Dawson G, Chen W (2011) Simple pyrolysis of urea into graphitic carbon nitride with recyclable adsorption and photocatalytic activity. J Mater Chem 21:14398-14401. https://doi.org/10.1039/C1JM12620B

26. Liu Y, Yuan A, Xiao Y, Yu H, Dong X (2020) Two-dimensional/two-dimensional Z-scheme photocatalyst of graphitic carbon nitride/bismuth vanadate for visible-light-driven photocatalytic synthesis of imines. Ceram Int 46: 16157-16165. https://doi.org/10.1016/j.ceramint.2020.03.171
27. Lucarelli L, Nadtochenko V, Kiwi J (2000) Environmental photochemistry: quantitative adsorption and FTIR studies during the TiO_2-photocatalyzed degradation of orange II. Langmuir 16:1102-1108. https://doi.org/10.1021/la990272j
28. Majumdar A, Pal A (2020) Recent advancements in visible-light-assisted photocatalytic removal of aqueous pharmaceutical pollutants. Clean Technol Environ Policy 22:11-42. https://doi.org/10.1007/s10098-019-01766-1
29. Mohazzab BF, Jaleh B, Issaabadi Z, Nasrollahzadeh M, Varma RS (2019a) Stainless steel mesh-GO/Pd NPs: catalytic applications of Suzuki–Miyaura and Stille coupling reactions in eco-friendly media. Green Chem 21:3319-3327. https://doi.org/10.1039/C9GC00889F
30. Mohazzab BF, Jaleh B, Nasrollahzadeh M, Issaabadi Z, Varma RS (2019b) Laser ablation-assisted synthesis of GO/TiO_2/Au nanocomposite: Applications in $K_3[Fe(CN)_6]$ and Nigrosin reduction. Mol Catal 473:110401. https://doi.org/10.1016/j.mcat.2019.110401
31. Mohazzab BF, Jaleh B, Nasrollahzadeh M, Khazalpour S, Sajjadi M, Varma RS (2020) Upgraded Valorization of Biowaste: Laser-Assisted Synthesis of Pd/Calcium Lignosulfonate Nanocomposite for Hydrogen Storage and Environmental Remediation. ACS omega 5:5888-5899. https://doi.org/10.1021/acsomega.9b04149
32. Nasri A, Jaleh B, Khazalpour S, Nasrollahzadeh M, Shokouhimehr M (2020) Facile synthesis of graphitic carbon nitride/chitosan/Au nanocomposite: A catalyst for electrochemical hydrogen evolution. Int J Biol Macromol 164: 3012-3024. https://doi.org/10.1016/j.ijbiomac.2020.08.143
33. Nasrollahzadeh M, Jaleh B, Baran T, Varma RS (2020a) Efficient degradation of environmental contaminants using Pd-RGO nanocomposite as a retrievable catalyst. Clean Technol Environ Policy 22:325-335. https://doi.org/10.1007/s10098-019-01784-z
34. Nasrollahzadeh M, Nezafat Z, Gorab MG, Sajjadi M (2020b) Recent progresses in graphene-based (photo) catalysts for reduction of nitro compounds. Mol Catal 484:110758. https://doi.org/10.1016/j.mcat.2019.110758
35. Nasrollahzadeh M, Shafiei N, Eslamipanah M, Fakhri P, Jaleh B, Orooji Y, Varma RS (2020c) Preparation of Au nanoparticles by Q switched laser ablation and their application in 4-nitrophenol reduction. Clean Technol Environ Policy. https://doi.org/10.1007/s10098-020-01899-8
36. Niu P, Zhang L, Liu G, Cheng HM (2012) Graphene-like carbon nitride nanosheets for improved photocatalytic activities. Adv Funct Mater 22:4763-4770. https://doi.org/10.1002/adfm.201200922
37. Ong W-J, Tan L-L, Ng YH, Yong S-T, Chai S-P (2016) Graphitic carbon nitride (g-C_3N_4)-based photocatalysts for artificial photosynthesis and environmental remediation: are we a step closer to achieving sustainability? Chem rev 116:7159-7329. https://doi.org/10.1021/acs.chemrev.6b00075
38. Orooji Y, Ghanbari M, Amiri O, Salavati-Niasari M (2020) Facile fabrication of silver iodide/graphitic carbon nitride nanocomposites by notable photo-catalytic performance through sunlight and

antimicrobial activity. J Hazard Mat 389:122079. https://doi.org/10.1016/j.jhazmat.2020.122079

39. Salavati-Niasari M (2005) Nanoscale microreactor-encapsulation of 18-membered decaaza macrocycle nickel (II) complexes. Inorg Chem Commun 8:174-177. https://doi.org/10.1016/j.inoche.2004.11.004
40. Salavati-Niasari M, Banitaba S (2003) Alumina-supported Mn (II), Co (II), Ni (II) and Cu (II) bis (2-hydroxyanil) acetylacetone complexes as catalysts for the oxidation of cyclohexene with tert-butylhydroperoxide. J Mol Catal A Chem 201:43-54. https://doi.org/10.1016/S1381-1169(03)00128-6
41. Salavati-Niasari M, Davar F, Fereshteh Z (2009a) Synthesis and characterization of ZnO nanocrystals from thermolysis of new precursor. Chem Eng J 146:498-502. https://doi.org/10.1016/j.cej.2008.09.042
42. Salavati-Niasari M, Davar F, Mazaheri M (2009b) Synthesis and characterization of ZnS nanoclusters via hydrothermal processing from [bis (salicylidene) zinc (II)]. J Alloys Compd 470:502-506. https://doi.org/10.1016/j.jallcom.2008.03.048
43. Salavati-Niasari M, Hasanalian J, Najafian H (2004) Alumina-supported $FeCl_3$, $MnCl_2$, $CoCl_2$, $NiCl_2$, $CuCl_2$, and $ZnCl_2$ as catalysts for the benzylation of benzene by benzyl chloride. J Mol Catal A Chem 209:209-214. https://doi.org/10.1016/j.molcata.2003.08.027
44. Salavati-Niasari M, Shakouri-Arani M, Davar F (2008) Flexible ligand synthesis, characterization and catalytic oxidation of cyclohexane with host (nanocavity of zeolite-Y)/guest (Mn (II), Co (II), Ni (II) and Cu (II) complexes of tetrahydro-salophen) nanocomposite materials. Microporous Mesoporous Mater 116:77-85. https://doi.org/10.1016/j.micromeso.2008.03.015
45. Tayel A, Nasr P, Sewilam H (2019) Forward osmosis desalination using pectin-coated magnetic nanoparticles as a draw solution. Clean Technol Environ Policy 21:1617-1628. https://doi.org/10.1007/s10098-019-01738-5
46. Venkateswarlu K, Bose AC, Rameshbabu N (2010) X-ray peak broadening studies of nanocrystalline hydroxyapatite by Williamson–Hall analysis. Physica B Condens Matter 405:4256-4261. https://doi.org/10.1016/j.physb.2010.07.020
47. Wahab R, Khan F, Al-Khedhairy AA (2018) Hematite iron oxide nanoparticles: apoptosis of myoblast cancer cells and their arithmetical assessment. RSC adv 8:24750-24759. https://doi.org/10.1039/C8RA02613K
48. Wang K, Li Q, Liu B, Cheng B, Ho W, Yu J (2015a) Sulfur-doped g-C_3N_4 with enhanced photocatalytic CO_2-reduction performance. Appl Catal B 176:44-52. https://doi.org/10.1016/j.apcatb.2015.03.045
49. Wang M, Cui S, Yang X, Bi W (2015b) Synthesis of g-C_3N_4/Fe_3O_4 nanocomposites and application as a new sorbent for solid phase extraction of polycyclic aromatic hydrocarbons in water samples. Talanta 132:922-928. https://doi.org/10.1016/j.talanta.2014.08.071
50. Yang X, Yang M, Pang B, Vara M, Xia Y (2015) Gold nanomaterials at work in biomedicine. Chem rev 115:10410-10488. https://doi.org/10.1021/acs.chemrev.5b00193

51. Zhang D, Liu J, Li P, Tian Z, Liang C (2017) Recent Advances in Surfactant-Free, Surface-Charged, and Defect-Rich Catalysts Developed by Laser Ablation and Processing in Liquids. ChemNanoMat 3:512-533. https://doi.org/10.1002/cnma.201700079
52. Zhang Y, Liu J, Wu G, Chen W (2012) Porous graphitic carbon nitride synthesized via direct polymerization of urea for efficient sunlight-driven photocatalytic hydrogen production. Nanoscale 4:5300-5303. https://doi.org/10.1039/C2NR30948C
53. Zhu H-Y, Xiao L, Jiang R, Zeng G-M, Liu L (2011) Efficient decolorization of azo dye solution by visible light-induced photocatalytic process using SnO_2/ZnO heterojunction immobilized in chitosan matrix. Chem eng j 172:746-753. https://doi.org/10.1016/j.cej.2011.06.053
54. Zhu J, Xiao P, Li H, Carabineiro SA (2014) Graphitic carbon nitride: synthesis, properties, and applications in catalysis. ACS Appl Mater Interfaces 6:16449-16465. https://doi.org/10.1021/am502925j
55. Zhuang Y-T, Zhu T-T, Ruan M, Yu Y-L, Wang J-H (2017) A 2D porous Fe_2O_3/graphitic-C_3N_4/graphene ternary nanocomposite with multifunctions of catalytic hydrogenation, chromium (VI) adsorption and detoxification. J MaterChem A 5:3447-3455. https://doi.org/10.1039/C6TA09774J

Figures

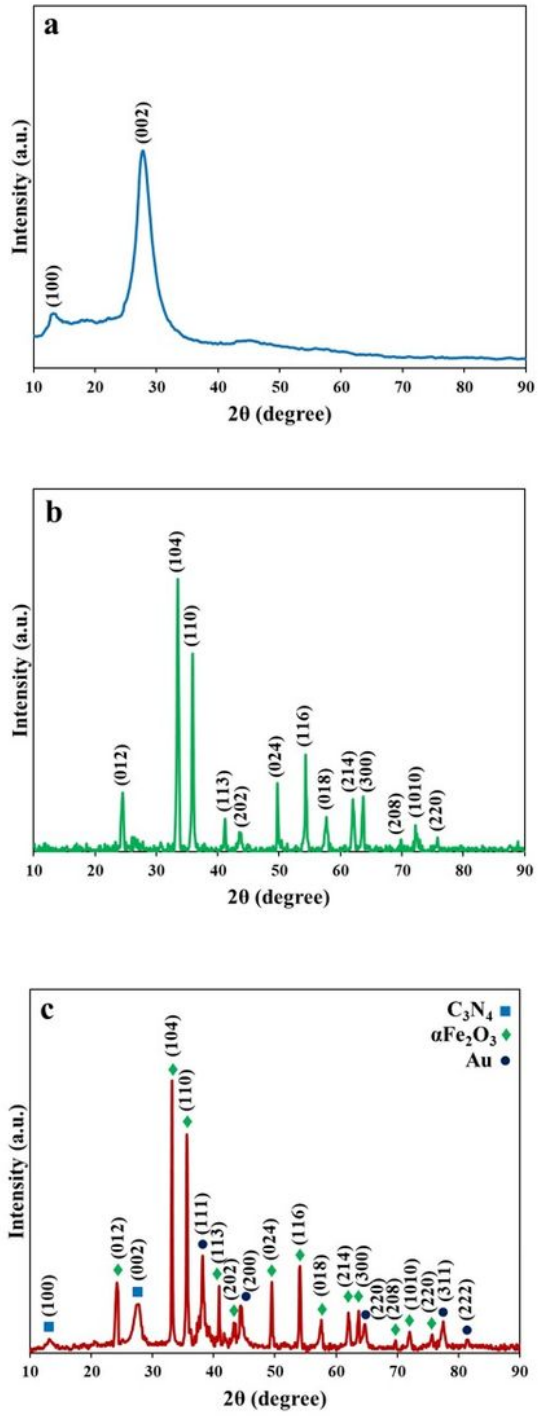

Figure 1

XRD spectra of C3N4 (a), Fe2O3 (b), and C3N4/Fe2O3/Au nanocomposite (c).

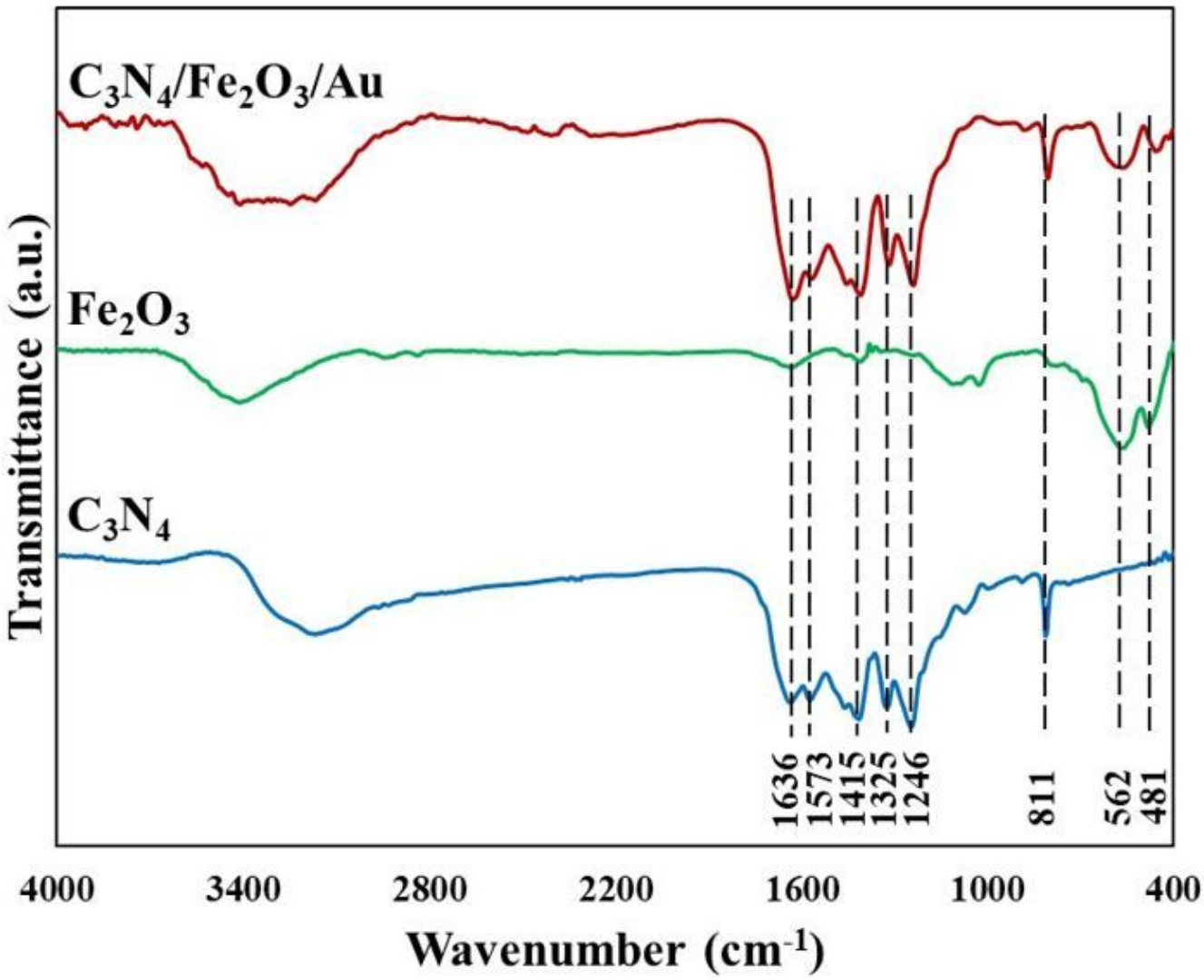

Figure 2

FTIR spectra of C3N4, Fe2O3, and C3N4/Fe2O3/Au nanocomposite.

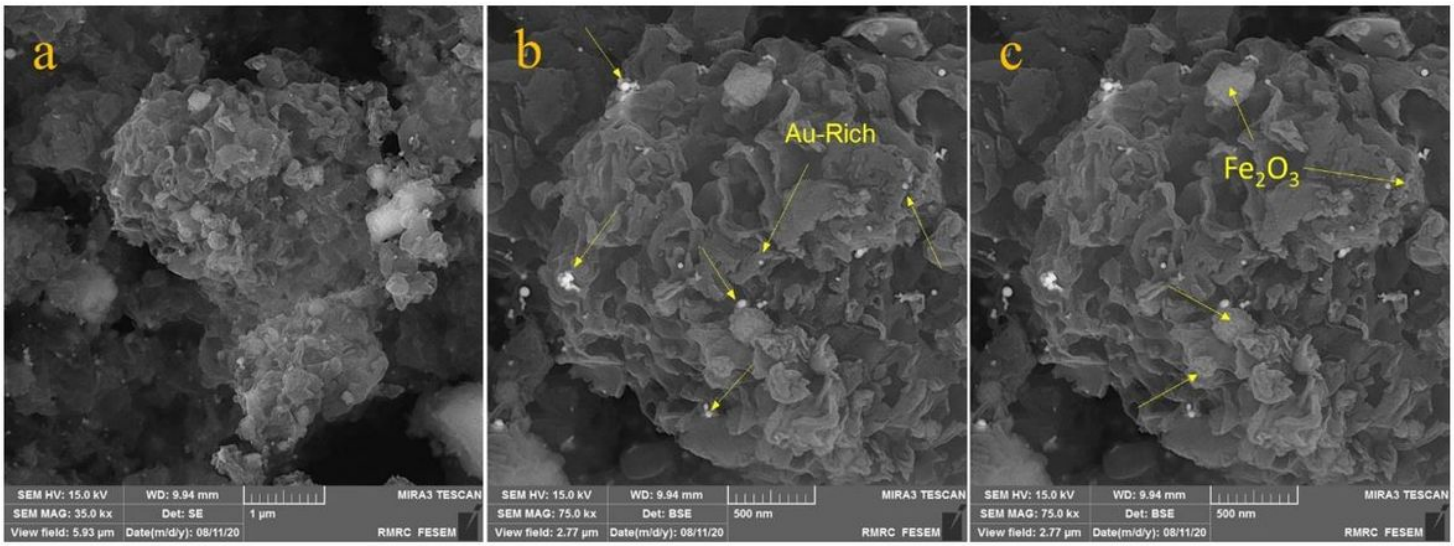

Figure 3

FESEM descriptions of C3N4/Fe2O3/Au.

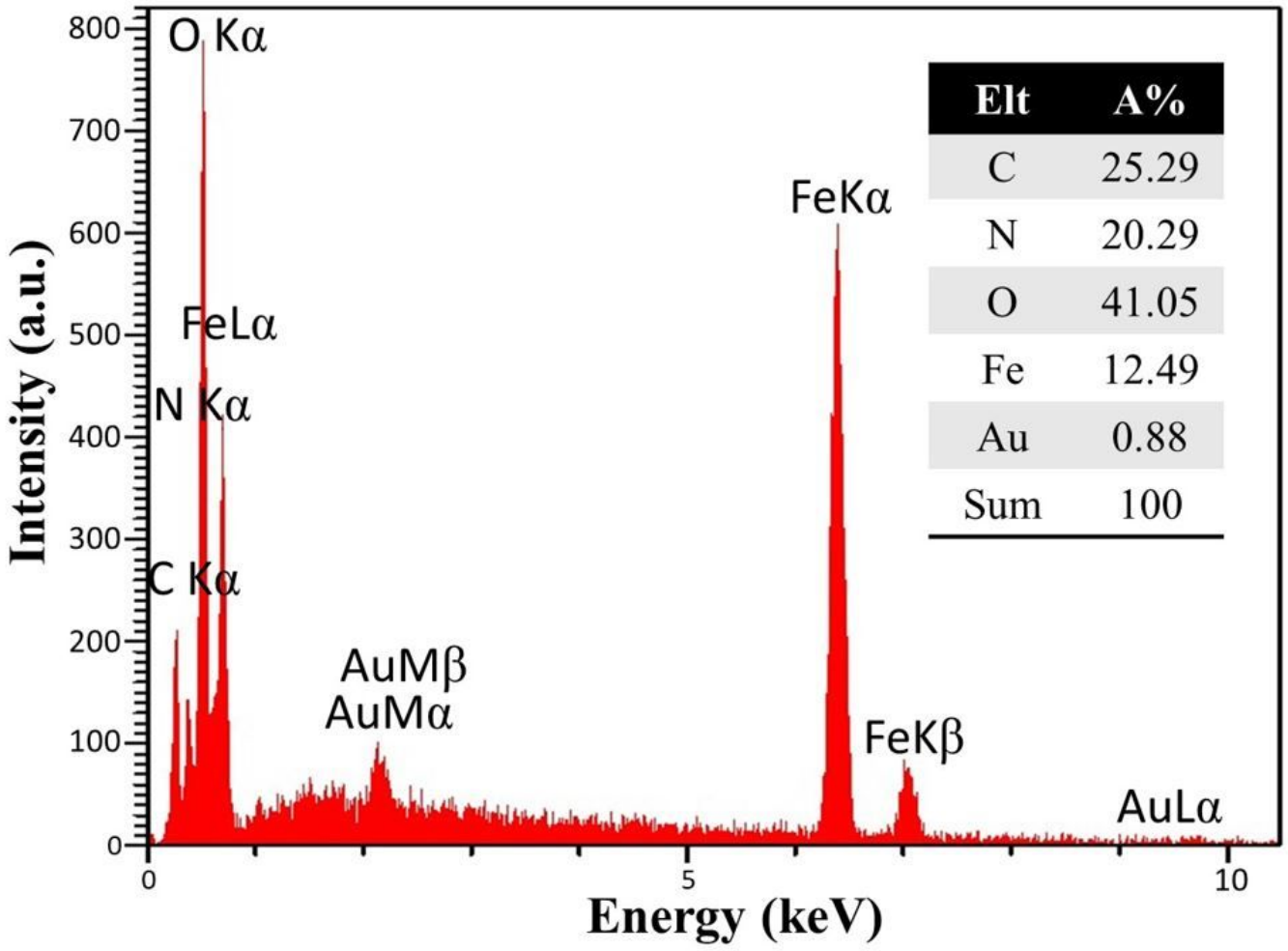

Elt	A%
C	25.29
N	20.29
O	41.05
Fe	12.49
Au	0.88
Sum	100

Figure 4

EDX spectrum of C3N4/Fe2O3/Au.

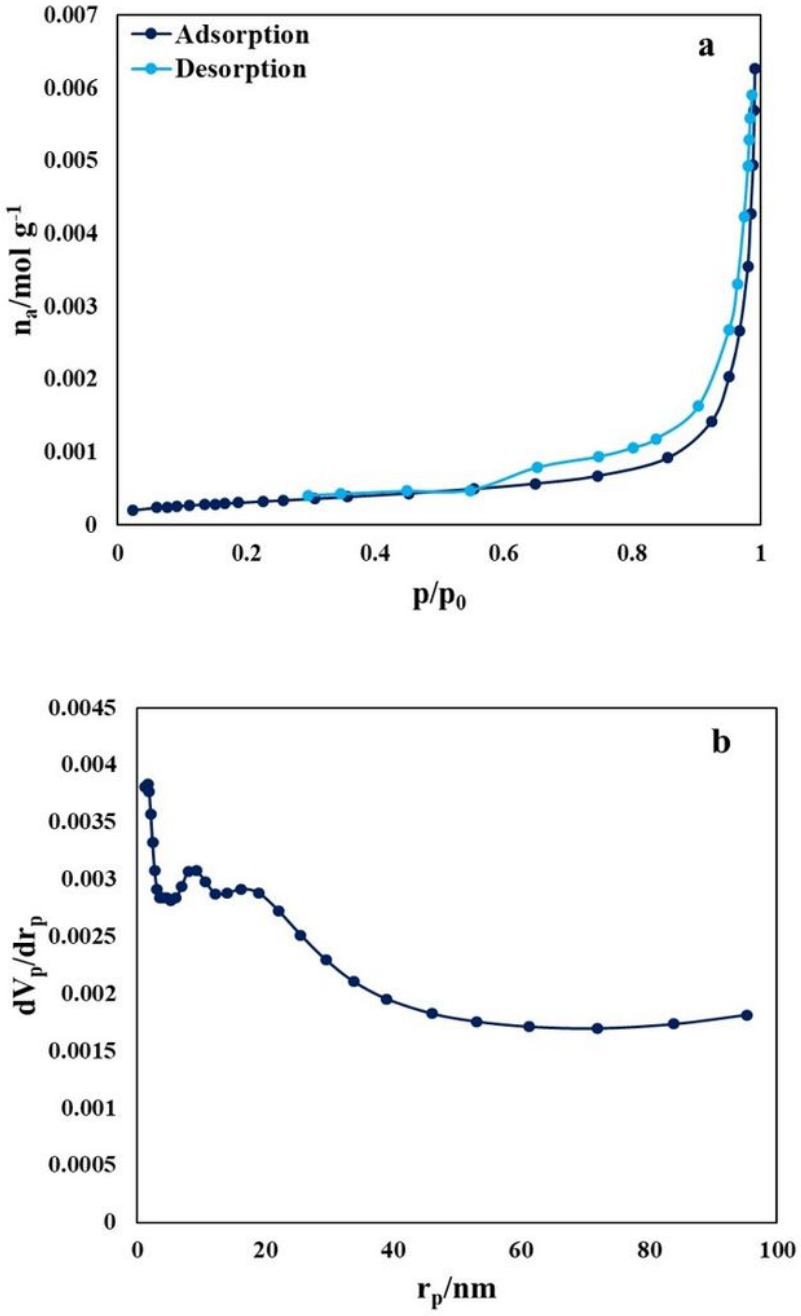

Figure 5

The adsorption-desorption of N2 isotherms (a) and pore size distribution (b) of C3N4/Fe2O3/Au.

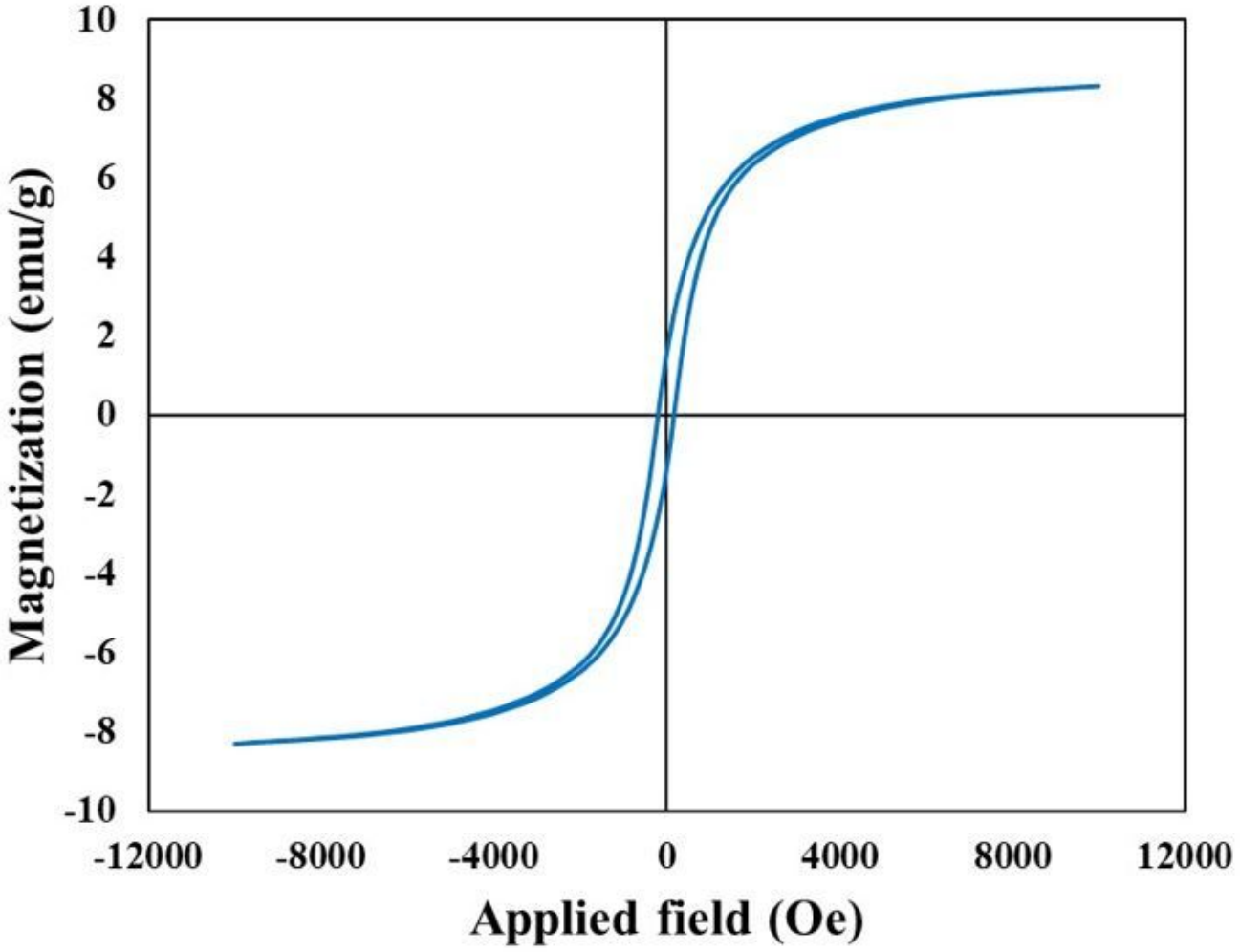

Figure 6

Room temperature magnetic hysteresis loop of C3N4/Fe2O3/Au.

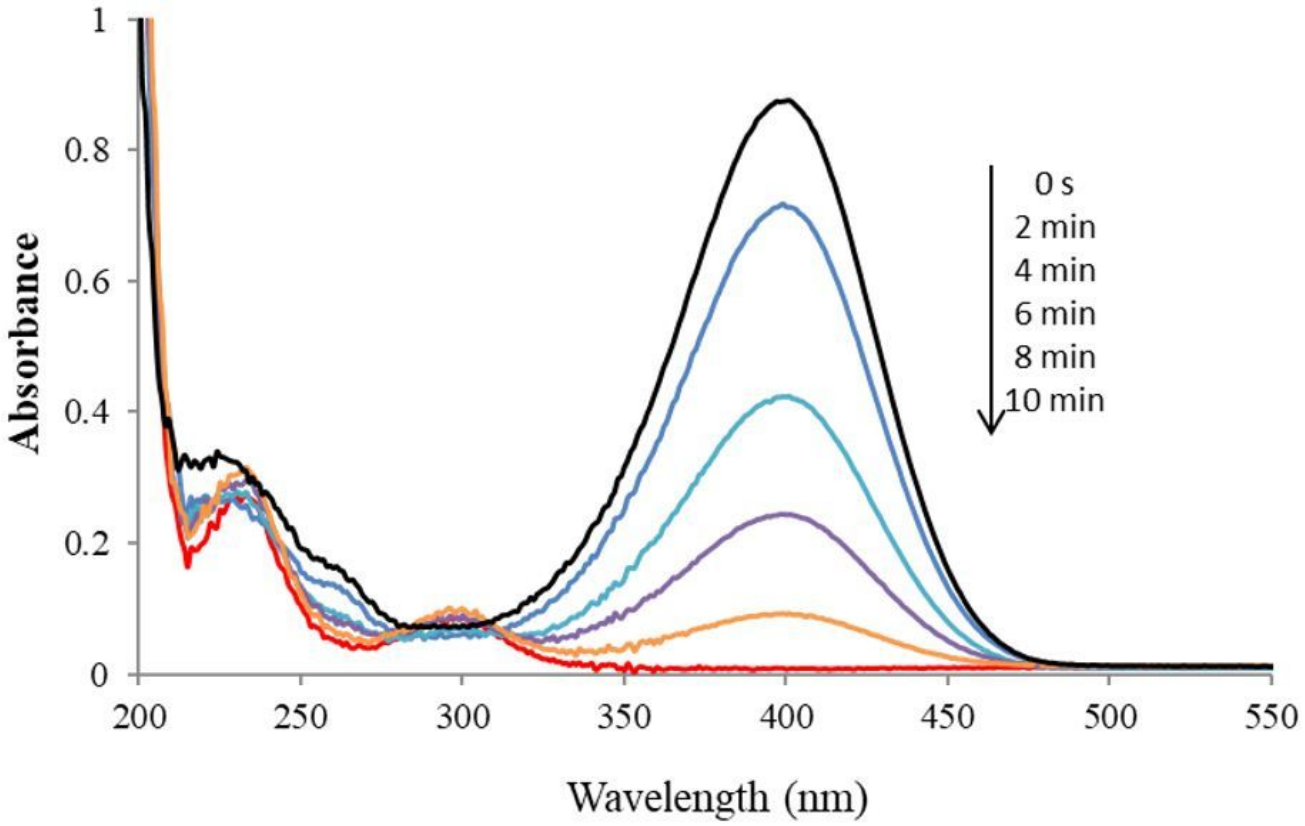

Figure 7

Variations in 4-NP UV-Vis spectra with time for the duration of reaction by 10 mg of C3N4/Fe2O3/Au.

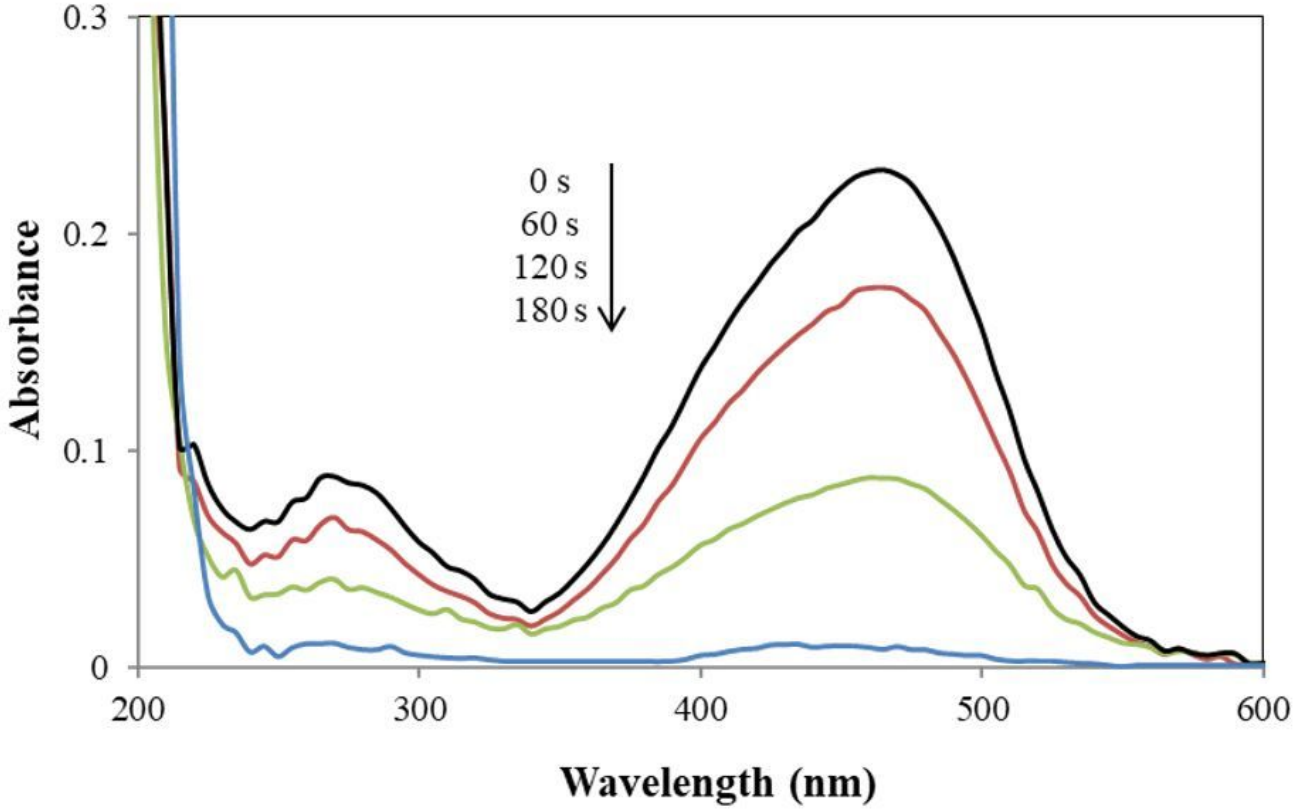

Figure 8

Variations in MO UV-Vis spectra with time for the duration of the reaction by 10 mg of C3N4/Fe2O3/Au.

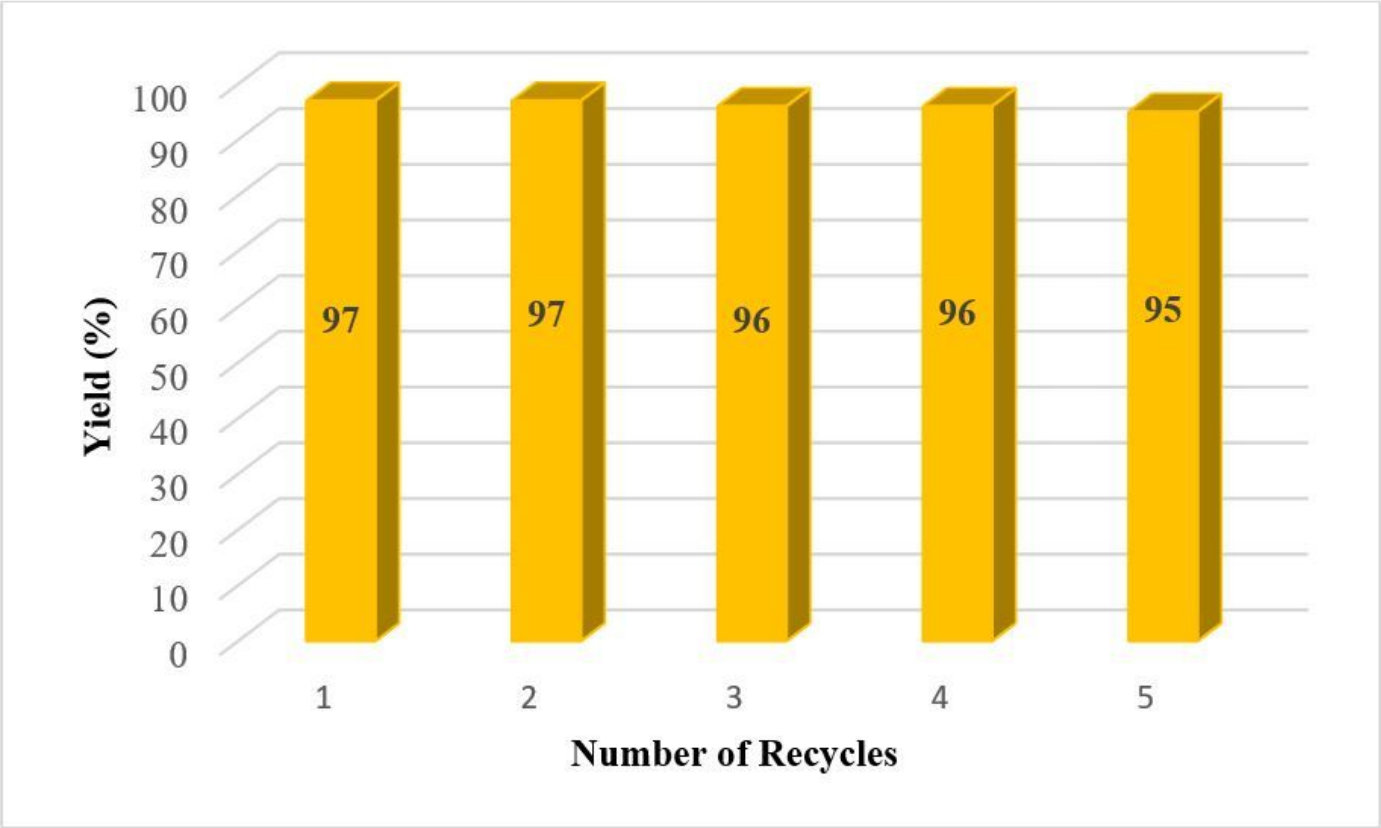

Figure 9

Recyclability potential of the C3N4/Fe2O3/Au nanocomposite in 4-NP reduction.

Supplementary Files

This is a list of supplementary files associated with this preprint. Click to download.

- Scheme1.jpg
- Scheme2.jpg
- Scheme3.jpg